Journal of Materials Chemistry

Dynamic Article Links

Cite this: *J. Mater. Chem.*, 2012, **22**, 14518

www.rsc.org/materials

PAPER

Crosslinkable liquid crystalline copolymers with variable isotropization temperature†

Kelly A. Burke‡[ab] and Patrick T. Mather*[bc]

Received 9th May 2012, Accepted 1st June 2012
DOI: 10.1039/c2jm32938g

Main-chain liquid crystalline polymers were synthesized from diene mesogens using acyclic diene metathesis polymerization to control the thermal properties of an unsaturated polymer that may subsequently be crosslinked to form nematic networks. The mesogen homopolymer forms a nematic phase with a glass transition of 74 °C and an isotropization temperature of 189 °C. Copolymerizing the mesogenic monomer with a more flexible, nonmesogenic monomer lowered the temperatures of the glass and isotropization (clearing) transitions and decreased the latent heat of the clearing transition. The unsaturated backbone of the polymers may be crosslinked using a free-radical initiator, and this was demonstrated for a selected composition. The early stages of the crosslinking reaction were found to obey a first-order rate law, with rate constants that depended on temperature in an Arrhenius manner (E_a = 118.9 kJ mol^{-1}). Measurement of the shear storage and loss moduli using a rotational rheometer during crosslinking showed that free-radical crosslinking can be used to prepare a liquid crystalline network with a subambient glass transition temperature.

Introduction

Thermotropic liquid crystalline polymers (TLCP) are polymers that form orientationally ordered phases in the molten state, leading to lower melt viscosities and improved mechanical properties over non-liquid crystalline polymers as well as the possibility of forming oriented materials.[1,2] Mesogens are the rigid molecules that drive the formation of ordered phases above the melting transition of TLCPs, and the stability of such phases is characterized by an isotropization temperature and an associated endothermic latent heat. Not all rigid molecules will form liquid crystalline phases, and calamitic mesogens with larger aspect ratios generally form more stable liquid crystalline phases having larger latent heats and isotropization temperatures. While researchers seek to maximize stability of the liquid crystalline phase, the achievement of an isotropization temperature lower than the onset of decomposition is desirable so as to afford erasure of liquid crystalline texture history[3–7] and the orientational benefits of flow-induced liquid crystallinity.

Although increasing the rigidity of a thermotropic liquid crystalline polymer chain facilitates the formation of the ordered phase, a common problem is that the melting temperatures of the TLCPs can exceed their decomposition temperatures. Methods used to decrease the polymer's melting temperature may be classified into the following categories: the use of mesogens with bulky,[8–13] polar,[1,12,14,15] or flexible side chains,[1,9,10,16–24] the insertion of rigid bent (nonmesogenic) comonomers[1,9,24–28] or flexible comonomers[1,9,10,16–24] that introduce a "kink" into or decrease the rigidity of the polymer chain, and the copolymerization of a mesogen with one or more distinct monomers. Homopolymers of mesogens with the bulky *tert*-butyl substituent have even been shown to suppress crystallization entirely, yielding a broad nematic phase above the glass transition.[13] Copolymerization of mesogenic monomers with other molecules, flexible or rigid, aids in tailoring the melting and clearing temperatures of the resulting polymer because, in addition to the effects contributed by the comonomer (ex. different substituents or increased flexibility), the liquid crystallinity of a copolymer may be affected by monomer sequence. In general, a regular copolymer sequence favors close packing of the polymer chains leading to a higher degree of crystallinity, larger and more perfect crystals, and sharper melting transitions that occur at higher

[a]*Department of Macromolecular Science and Engineering, Case Western Reserve University, Cleveland, OH, USA*
[b]*Syracuse Biomaterials Institute, Syracuse, NY, USA*
[c]*Department of Biomedical and Chemical Engineering, Syracuse, NY, USA. E-mail: ptmather@syr.edu*

† Electronic supplementary information (ESI) available: (1) ^{1}H NMR spectra of **P5tB(100)**, **P5tB(0)**, and **P5tB(81.1)**. (2) Free radical crosslinking of **P5tB(97.3)** with 10 wt% lauroyl peroxide, including plots of ln(1 − *p*) *versus* cure time *t* to determine temperature-dependent rate constants (*k*(*T*)) and a plot of *k*(*T*) *versus* 1/*T* to determine activation energy of the cure. (3) Free radical crosslinking of **P5tB(97.3)** with 5.16 wt% lauroyl peroxide. Shown is the the plot of ln(1 − *p*) *versus* cure time *t* for the cure at 60 °C, which was studied to determine the rate constant, *k*, for this cure. See DOI: 10.1039/c2jm32938g

‡ Present address: Department of Biomedical Engineering, Tufts University, Medford, MA, USA.

temperatures.[1,29–33] Though TLCPs may be tailored by any one or combination of these methods, these methods that decrease the temperature of the melting and clearing transitions also decrease liquid crystalline order.[34]

Liquid crystalline polymers may be crosslinked to give liquid crystalline networks (LCNs). Liquid crystalline networks are classified by the way in which the mesogens are incorporated into the network: main-chain, in which the mesogen is incorporated directly into the network chains, and side-chain, in which the mesogens are attached as pendent groups onto the network chains by a short spacer. Common applications of liquid crystalline thermosets include the toughening of resins,[35–38] as well as the production of ordered networks with azobenzene dyes for nonlinear optical applications.[39,40] Due to a coupling of orientational order and strain, LCNs have also been envisaged for actuation applications in which the heat-induced switching between an ordered liquid crystalline phase and the isotropic phase is converted to mechanical work by the polymer.[41–47] In principle, the main-chain network is more desirable for actuation, as its phase behavior is closely coupled to macroscopic network strain.[47] Tokita and coworkers[46] have shown, quite surprisingly, actuation in a glassy monodomain nematic polyester network, where the material contracts upon heating and elongates upon cooling under applied stress, thus yielding reversible contractile actuation. Similar actuation behavior has been observed in main-chain siloxane-based smectic liquid crystalline elastomers (LCEs).[42,48–50] In addition to their actuation properties, these networks are attractive for their excellent shape memory fixing and recovery properties.[48,50] These interesting properties of main-chain smectic elastomers motivated work to develop a *nematic* main-chain elastomer.

Architecturally, networks formed from segmented polymers or by crosslinking at well-defined sites will tend to stratify into layered phases, whereas crosslinking randomly along a uniform (nonsegmented) polymer chain will form networks with no propensity to form layered phases due to the disorder that arises from a distribution of chain lengths between crosslink points. As an example, our group has previously shown that siloxane-based segmented main-chain LCP[51] and LCEs[48,50] feature a smectic phase intrinsic to their architecture, but homopolymers prepared from the same mesogen form only the nematic phase before isotropization.[52] To achieve the goal of a nematic main-chain elastomer, an alternate synthetic scheme involving random crosslinking of nonsegmented copolymers was developed. This manuscript describes the preparation of nematic liquid crystalline networks (LCNs) using a two reaction approach. Diene monomers were first polymerized using acyclic diene metathesis (ADMET) chemistry[53] to produce unsaturated liquid crystalline polymers, which were subsequently crosslinked using a free-radical initiator. This two-step synthesis allows the tailoring and characterization of the polymer's properties prior to crosslinking. This manuscript focuses first on controlling the phase behavior of a polymer by copolymerizing a liquid crystalline diene monomer with a comparatively flexible, yet aromatic, diene comonomer using ADMET chemistry. The residual unsaturation of the LCPs was then exploited by a crosslinking reaction that allowed preparation of the desired main-chain liquid crystalline network.

Experimental

Reagents

Terephthaloyl chloride (99%), anhydrous pyridine (99.8%), 4-penten-1-ol (99%), 4 hydroxybenzoic acid (99%), 5-bromo-1-pentene (95%), *tert*-butyl hydroquinone (97%), 1,3-dicyclohexylcarbodiimide (99%), 4-(dimethylamino)pyridine (99%), potassium carbonate (anhydrous, 99.7%), potassium hydroxide (≥90%), lauroyl peroxide (Luperox LP, 97%), 3-bromopyridine (99%), and deuterated chloroform (99.8 atom% D) were purchased from Aldrich. Grubbs' first and second generation catalysts were also purchased from Aldrich, but no information regarding purity was supplied. Grubbs' third generation catalyst was synthesized from the second generation catalyst as previously reported[54] and used without further purification. Anhydrous tetrahydrofuran (THF) (99.9%) and ethyl vinyl ether (99%) were obtained from Acros. Tris(hydroxymethyl)phosphine (95%) was purchased from Strem Chemicals. Hydrochloric acid (ACS Plus grade) and all other solvents were purchased from Fisher Scientific. All chemicals were used without further purification, with the exception of *tert*-butyl hydroquinone, which was recrystallized from toluene (approximately 20 g L^{-1}) to yield white crystals.

Synthesis of 2-*tert*-butyl-1,4-phenyl(bis(4-pentenyloxybenzoate)) (5tB)

The synthesis of **5tB**, the liquid crystalline monomer, was adopted from literature.[51] The yield after purification was about 50%. ^{1}H NMR in $CDCl_3$ gave δ in ppm: 8.16 (4H, m), 7.24 (1H, d), 7.12 (2H, t), 6.99 (4H, m), 5.87 (2H, m), 5.06 (4H, m), 4.07 (4H, t), 2.27 (4H, m), 1.94 (4H, m), 1.38 (9H, s). This monomer has a glass transition at −9.40 °C (0.276 J g^{-1} °C^{-1})) upon heating, and this is followed by a weak melting endotherm at 79.4 °C (1.24 J g^{-1}) and an isotropization endotherm at 89.3 °C (3.57 J g^{-1}).

Synthesis of 1,4-bis(pent-4-enyl) benzoate (5Te)

The preparation of 1,4-bis(pent-4-enyl) benzoate (**5Te**), the nonmesogenic diene monomer, followed a procedure modified from the literature.[55] Terephthaloyl chloride (10.0 g, 0.0492 mol) was weighed into a flame-dried three-neck round bottomed flask and purged with nitrogen gas for 30 min. Anhydrous THF (60 mL) was added to the flask, followed by the addition of anhydrous pyridine (8 mL, 0.0989 mol). Finally, 4-penten-1-ol (10.2 mL, 0.0988 mol) was added in slight excess to the reaction to ensure a disubstituted product. The reaction proceeded for 4 h at 70 °C, after which the THF was removed by rotary evaporation to yield a white solid. The solids were dissolved in distilled water and extracted with hexanes three times. The aqueous phase was removed and discarded, while the organic phase was washed with 1 M HCl. Again, the aqueous phase was discarded, and the organic phase was washed three times with an aqueous solution of K_2CO_3 (0.7 M). The organic phase was then washed with distilled water until the pH of the aqueous phase was about 6. The impure product, a yellow oil, was isolated from the organic phase by rotary evaporation and dried overnight under vacuum at 30 °C. Purification of the dried product was achieved by

recrystallization from 2-propanol. The yield after recrystallization was found to be about 62%. ^{1}H NMR in $CDCl_3$ gave δ in ppm: 8.12 (4H, s), 5.72–5.97 (2H, m), 5.01–5.12 (4H, m), 4.35–4.39 (4H, t), 2.23–2.25 (4H, q), 1.88–1.93 (4H, p). The melting temperature of this monomer is 32.6 °C, and no other thermal transitions were observed upon heating, confirming the expectation that **5Te** is not liquid crystalline.

Synthesis of homopolymers and copolymers with Grubbs' first generation catalyst

As an example, the synthesis described here is an ADMET polymerization with 95 mol% **5tB** and 5 mol% **5Te** in the feed of the reaction. Qin's work on the polymerization of **5tB** using various catalysts served as a starting point for the design of this polymerization procedure.[52] Here, the procedure was modified to include continuous purging of ethylene gas, a reaction by-product, by a nitrogen stream as well as measures to reduce solvent loss from the reaction. Removal of ethylene shifts the reaction equilibrium towards polymer formation, while slowing solvent loss kept the reactants in solution longer, both of which are thought to contribute to the formation of higher molecular weight polymers. It should be noted that the reaction conditions are the same for the homopolymers and the copolymers, and that only the monomer feed ratio was varied to give a range of polymer compositions.

In a nitrogen gas-charged glovebox, 0.0260 g (0.0860 mmol) **5Te**, 0.494 g (0.910 mmol) **5tB**, 0.0161 g (0.0196 mmol) Grubbs' first generation catalyst, 2.0 mL dry toluene, and a magnetic stir bar were added to a 50 mL Airfree® reaction flask (Chemglass Inc.). A dewar condenser was joined to the reaction flask, and the whole apparatus was sealed from the atmosphere by septum prior to removal from the glovebox to ensure that the atmosphere remained inert and dry. Once removed from the glovebox, the flask was placed in an oil bath and the reaction proceeded at 55 °C under flowing nitrogen gas for 9 h. The dewar condenser was charged with acetone and dry ice, which was periodically replenished, to slow the evaporation of toluene. The reaction was then diluted by the addition of 5.0 mL of toluene, terminated by the addition of 0.57 mL ethyl vinyl ether (about 300 molar excess ethyl vinyl ether relative to catalyst), and stirred at 40 °C for 30 min. Residual ruthenium complexes were removed by adding at least 25 moles of tris(hydroxymethyl)phosphine (THMP) per mole of catalyst. In this case, 0.35 mL of a 1.8 M solution of THMP in 2-propanol was added and allowed to stir for 24 h at 40 °C. Finally, the solution was added dropwise to a methanol–distilled water mixture (9/1 v/v), from which a white precipitate formed. The precipitate was isolated by vacuum filtration and dried overnight at 40 °C. Yield of the precipitated polymer was greater than 50%, noting that some low molecular weight species may have been lost in the precipitation step. After drying under vacuum, ^{1}H NMR was used to determine the composition of the copolymers. The polymers are named as **P5tB(*xx*)**, where *xx* denotes the mole percent of **5tB** incorporated in the polymers as measured by ^{1}H NMR. Spectra are available in ESI†.

All polymers in this manuscript were prepared in this manner except for the polymer used to demonstrate crosslinking, **P5tB(97.3)-G3**. As will be shown, **P5tB(97.3)-G3**, was synthesized without the use of a glovebox and employed Grubbs' third generation catalyst (**G3**). Grubbs' third generation catalyst initiates faster than Grubbs' first generation catalyst (**G1**), and it was thought that polymers synthesized using **G3** would have larger molecular weights than polymers produced using **G1** in these conditions.

Synthesis of copolymers with Grubbs' third generation catalyst

This polymerization was modified from the work of McKenzie *et al.*[56] and employed Grubbs' third generation catalyst (**G3**), which was easily prepared from Grubbs' second generation catalyst.[54] The **G3** catalyst (205.4 mg, 0.231 mmol), **5tB** (2.70 grams, 4.98 mmol), and **5Te** (74.4 mg, 0.246 mmol) were weighed into a flame dried and inert gas cooled 50 mL Airfree® reaction flask. The solids were then purged with nitrogen gas for 30 min. Distilled dichloromethane was degassed by bubbling nitrogen gas through the solvent for several minutes before 16 mL (**5tB** concentration was 311 mM) was added to the reaction. The headspace was evacuated for 30 s using a vacuum line while nitrogen gas was bubbled through the solvent. The reactor was then sealed at ambient pressure to preserve the N_2 atmosphere, following which the reaction was allowed to proceed at room temperature with magnetic stirring for 4 h. Every 10 min for the first hour the vacuum/purge process was repeated to remove ethylene gas; thereafter it was repeated every 30 min. During this reaction, no noticeable increase in viscosity was observed. The reaction was terminated by ethyl vinyl ether, as described above. Tris(hydroxymethyl phosphine) (THMP) (25 mmol per mmol catalyst) was added to the reaction to remove residual ruthenium complexes, but this could not be separated from the polymer easily because the resulting polymer was apparently too low in molecular weight to precipitate from solution (see Results and Discussion). As a result, the THMP was removed by washing the polymer solids with water. While THMP is quite soluble in water and the washing steps were repeated, this method is inferior to precipitation and it is noted that residual THMP could be present in the polymer product, though signals due to THMP could not be detected using ^{1}H NMR. The yield of the polymer was 75.6%, and we postulate that this low yield was due to the washing steps required to remove THMP. This polymer is referred to as **P5tB(97.3)-G3** to denote that the polymer was synthesized using the Grubbs' third generation catalyst.

Characterization

Confirmation of chemical structures and composition of copolymers was achieved by liquid phase ^{1}H nuclear magnetic resonance (^{1}H NMR) spectroscopy using a Varian Gemini spectrometer operating at 300 MHz, Varian Unity Inova spectrometer operating at 600 MHz, or a Bruker Avance DPX300 spectrometer operating at 300 MHz. Samples were dissolved in $CDCl_3$ (10 mg mL^{-1}), and data were acquired at room temperature. MestReC software (version 4.8.6.0, Mestrelab Research S.L.) was used for spectra analysis.

Gel permeation chromatography (GPC) was used to determine the molecular weight (M_n and M_w) and polydispersity index of the polymers. Two GPC systems were used for this work, with all but one polymer analyzed using the Varian system installed at Case Western Reserve University. The Varian system consisted

of a set of three columns packed with crosslinked polystyrene in series: a MesoPore guard column (Polymer Laboratories) 5 cm in length with 3 μm pore size, a MesoPore column (Polymer Laboratories) 30 cm in length with 3 μm pore size, and finally a GMH_{HR}-M mixed-bed column (Tosoh Bioscience Inc.) 30 cm in length with 5 μm pore size. This GPC was equipped with a Varian ProStar Model 320 UV-Vis detector, a Varian ProStar Model 350 refractive index detector, and Viscotek Model 270 Dual Detector for viscosity and light scattering (both 7° and 90°) measurements. Absolute molecular weight was measured by in-line light scattering, and OmniSEC (version 3.1, Viscotek Corp.) was used to calculate molecular weights (M_n and M_w) and polydispersity of the polymers. The alternate GPC system was a Waters Isocratic HPLC system installed at Syracuse University. This system consisted of three columns in series: a 5 cm ResiPore© column, a 30 cm long ResiPore© column, and another 30 cm long ResiPore© column, each of which were purchased from Polymer Laboratories, Inc. and packed with 3 μm crosslinked polystyrene particles. This GPC was equipped with a Waters 2414 Refractive Index Detector and a Wyatt miniDAWN TREOS multi-angle light scattering detector (49°, 90°, and 131°). Absolute molecular weight was measured by in-line light scattering, and ASTRA software (version 5.3.4.15, Wyatt) was used to calculate molecular weights (M_n and M_w) and polydispersity of the polymers. For both systems, polymers were dissolved in HPLC-grade THF to give a concentration between 2 and 8 mg mL^{-1} and eluted through the columns at a flow rate of 1 mL min^{-1}.

Differential Scanning Calorimetry (DSC) experiments were performed on a TA Instruments Q100 (Case Western Reserve University) or Q200 (Syracuse University) DSC equipped with a refrigerated cooling system and calibrated using the TZero calibration procedure (TA Instruments-Waters LLC). Data were collected with Q Series Software (version 2.8.0.393) and analyzed using Universal Analysis Software (version 4.5.05) from TA Instruments-Waters LLC. All samples were run under flowing nitrogen atmosphere (50 mL min^{-1}) and were heated and cooled at 10 °C min^{-1} through the temperature range of −90 °C to 200 °C twice, with the first heating and cooling cycles employed to erase thermal history and the second heating and cooling cycles used to identify the material's transitions. This temperature range proved sufficient to analyze the glass transition and isotropization (clearing) transition of all the polymers in this study, with the exception of the **5tB** homopolymer. The isotropization temperature of this polymer is close to 200 °C, so this sample was heated to 210 °C in order to study the entire transition. The glass transition temperature was determined by taking the midpoint of the stepwise change in the heat flow signal from the second heating trace, whereas the isotropization (clearing) transition temperatures were found by taking the minimum of the peak from the second heating trace or the maximum of the peak from the second cooling trace. The latent heat of the clearing transition was also studied by setting integration limits where the heat flow signal departed from linearity, and subsequently integrating between these limits to find the area under the curve. For both the glass transition and the clearing transition, a minimum of four experiments were run for each sample so that the average with standard deviation are reported for each polymer.

Polarized light optical microscopy was used to identify the liquid crystalline phases of the polymers. For these experiments, an Olympus BX51 microscope was equipped with 90° crossed polarizers, a HCS402 hot stage from Instec Inc., and a digital camera (14.2 Color Mosaic Model from Diagnostic Instruments, Inc.). Images were acquired from the camera at selected temperatures using Spot software (Diagnostic Instruments, Inc.). Spatial dimensions were calibrated using a stage micrometer with 10 μm line spacing, and a 20×/0.4 NA achromat long working-distance objective lens (Olympus LMPlanFI) was employed. The samples used for POM analysis were dissolved in chloroform to give a 1 wt% solution which was then added dropwise to a clean microscope slide and covered to slow evaporation, which was taken to completion. The Instec hotstage was equipped with a liquid nitrogen LN_2-P cooling accessory for accurate temperature control during heating and cooling runs. To erase thermal history, the samples were heated to 200 °C, held at 200 °C for 1 min, cooled to −10 °C at 10 °C min^{-1}, held at −10 °C for 1 min, and finally heated to 25 °C at 10 °C min^{-1}. The samples were then heated to 200 °C at 10 °C min^{-1}, held at 200 °C for 1 min, and cooled to −10 °C at 10 °C min^{-1}. Optical micrographs were collected during these second heating and cooling runs.

Copolymer crosslinking with lauroyl peroxide

The kinetics of crosslinking the unsaturated double bonds in the backbone of **P5tB(97.3)-G3** with 10 wt% lauroyl peroxide was monitored using DSC. Lauroyl peroxide was selected because its initiation temperature is low, which permitted cure of **P5tB(97.3)-G3** at a temperature where the polymer's viscosity was sufficient to maintain a meniscus in rotational rheometry. Selection of this initiator thus permitted rheological monitoring of the cure, as described later. For the kinetics study, the blend of polymer and initiator were isothermally cured at a selected temperature. To prepare samples, **P5tB(97.3)-G3** was blended with 10 wt% lauroyl peroxide by dissolving the polymer and initiator in toluene and subsequently removing the solvent by rotary evaporation and vacuum drying at room temperature. Samples were encapsulated in aluminum DSC pans, heated to a selected cure temperature, and isothermally cured at this temperature. The blend was then cooled and heated back through the cure temperature, which completes the reaction. By measuring the residual heat of reaction measured during this heating step, the fraction of material cured during the isothermal hold can be calculated.[57] The thermal program for this study was as follows: the samples were heated at 40 °C min^{-1} to the curing temperature, held at this temperature for a specified amount of time, cooled at 40 °C min^{-1} to −50 °C, heated at 10 °C min^{-1} to 180 °C ("first heat after cure"), held for 1 min, cooled to −50 °C at 10 °C min^{-1}, held for 1 min, heated at 10 °C min^{-1} to 180 °C ("second heat after cure"), held for 1 min, and cooled to −50 °C at 10 °C min^{-1}. A minimum of six different curing times, varying between 0 and 180 min, were studied at four crosslinking temperatures: 60 °C, 70 °C, 80 °C, and 90 °C. The fractional extent of cure was ascertained using the expression:

$$p = 1 - \frac{\Delta H_{res}(T,t)}{\Delta H_o} \quad (1)$$

where $\Delta H_{res}(T,t)$ is the residual exothermic heat of reaction measured after crosslinking for time t at temperature T, and ΔH_o is the total exothermic heat of reaction measured on a sample whose cure time was 0 min. As defined, the fractional extent of cure, p, ranges from 0 for no crosslinking to 1 for complete crosslinking.

To demonstrate that the polymers crosslink to form networks during isothermal cure, the evolution of shear linear viscoelastic moduli of **P5tB(97.3)** was monitored using rotational rheometry. We anticipated that crosslinking of sufficient extent would lead to gelation, the point where the steady shear viscosity diverges and where a shear elastic modulus begins to grow.[58] Rheological experiments have shown that, at the gel point, the loss tangent (G''/G') becomes frequency-invariant and close to unity.[59,60] Here, gelation was studied using isothermal small angle oscillatory shear experiments, where the gel point was taken to be the point where the dynamic storage modulus crossed the dynamic loss modulus. While this would only coincide with the true gel point for the case where $\tan(\delta)_{gel} = 1$, we adopted this common practice owing to its simplicity. For these samples, the polymer was blended with lauroyl peroxide initiator in toluene, which was removed by room temperature rotary evaporation and by drying at room temperature under vacuum for at least 12 h. Because lauroyl peroxide forms gaseous by-products upon thermal decomposition, as is necessary to generate radicals, the amount of initiator was reduced from 10 wt% to 5.16 wt% to reduce the formation of these by-products, which may become trapped in the sample during crosslinking. The resulting blend was loaded into a TA Instruments AR G2 rheometer at 60 °C in between parallel plates (8 mm diameter). The solids were allowed to soften, as heat transferred to the sample, for about a minute, before the gap was decreased and excess polymer was trimmed away using a blade. Small angle oscillatory shear experiments were conducted at 1% strain and a frequency of 10 rad s^{-1}. The sample was maintained in a nitrogen atmosphere, and temperature was controlled using an oven and vaporized liquid nitrogen. Data were collected using Rheology Advantage (Version 5.7.0) and analyzed using Rheology Advantage Data Analysis (Version 5.7.0) from TA Instruments Ltd. to yield the time evolution of the shear storage and loss modulus.

Results and discussion

5Te was co-polymerized with **5tB** using ADMET chemistry and Grubbs' first generation catalyst according to Scheme 1. Comparing to previous reports,[52,57] the catalyst remained active for longer times in these reactions. The sustained activity was ascertained by the solution's bright, purple color and was attributed to our use of a continuous purge of inert gas. It is thought that the longer reaction time is why these polymers have higher molecular weights than those previously reported. The molecular weight and polydispersity index of the **5tB** homopolymer, the **5Te** homopolymer, and their copolymers are shown in Table 1. Also shown in this Table is the **5tB** composition in the feed of the reaction and incorporated into the polymer, as determined by ^{1}H NMR. The composition of the feed and polymer are quite close for all polymers, which suggests similar reactivity of the monomers. The weight-averaged molecular weight of all polymers synthesized for this study were between 23.7 and 31.4 kDa, and the polydispersity varied from 1.45 to 2.25. It should be noted that the PDI of these polymers as-synthesized could be slightly higher, as lower molecular weight species may have been removed in the workup by precipitation. The molecular weights and polydispersity indices of these polymers are thought to be sufficiently high and similar to allow the effect of polymer composition on the glass transition and isotropization transition to be studied without having to consider molecular weight effects on these transitions.

The thermal transitions of the polymers were studied using DSC and were found to be dependent on composition (Fig. 1). The traces are paired by material, where the bottom trace of each pair is the second heating run and the top trace of each pair is the

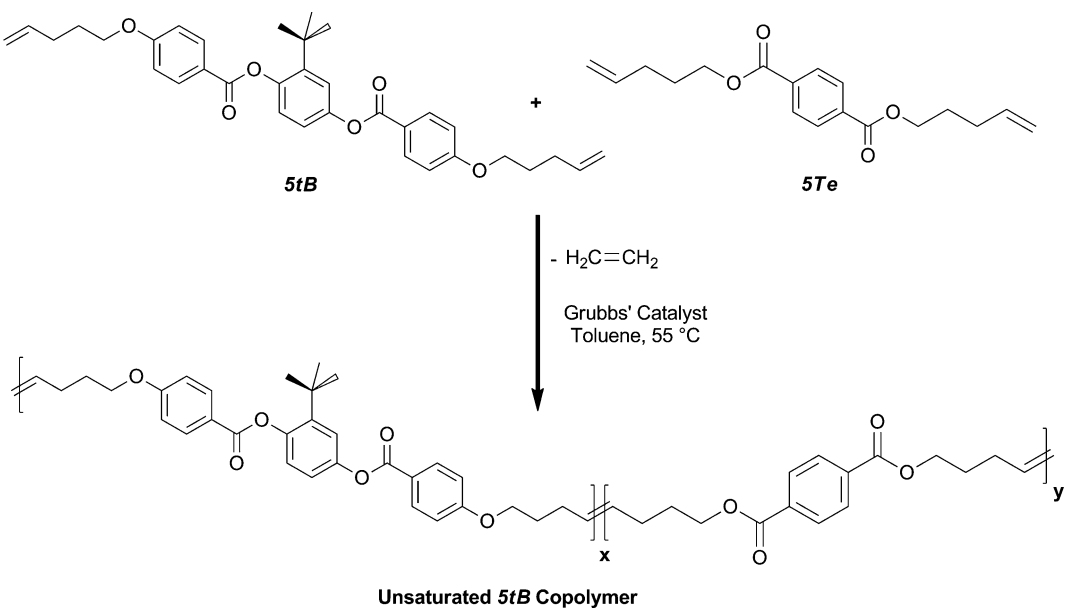

Scheme 1 Synthesis of liquid crystalline copolymers based on **5tB** and **5Te** by acyclic diene metathesis (ADMET) polymerization.

Table 1 Composition, weight-averaged and number-averaged molecular weight, and polydispersity of the polymers prepared by the route outlined in Scheme 1

5tB in polymer[a] (mol%)	**5tB** in feed (mol%)	M_w[b] (kDa)	M_n[b] (kDa)	PDI[b]
0.0	0	30.6	21.0	1.45
40.1	35.9	31.4	20.5	1.54
65.6	62.6	26.6	11.8	2.25
68.5	69.1	29.9	18.0	1.66
81.1	83.4	29.2	16.2	1.81
91.8	91.4	25.9	15.1	1.72
100.0	100.0	23.7	17.1	1.46

[a] As determined by ^{1}H NMR in $CDCl_3$. [b] As determined by GPC.

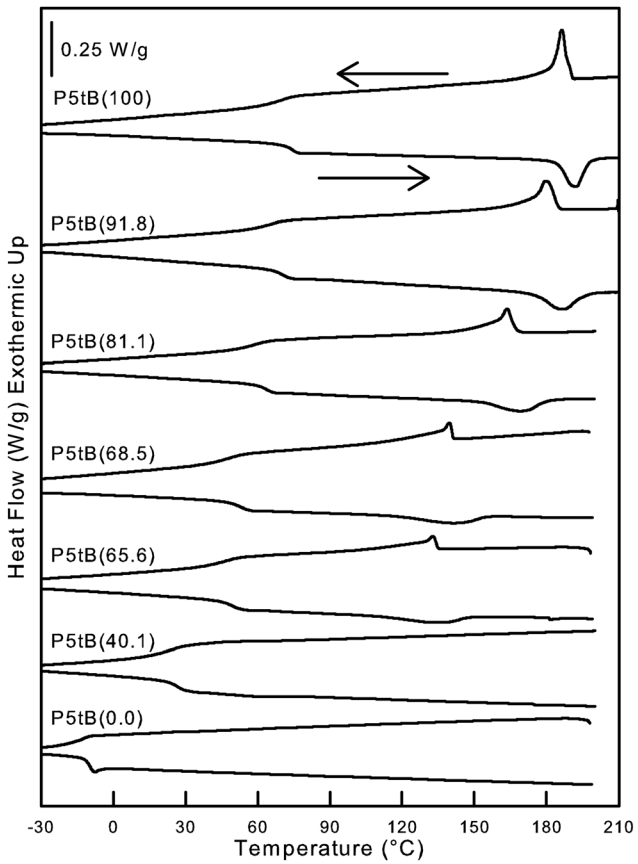

Fig. 1 Differential scanning calorimetry second heating and second cooling traces of the LCPs based on **5tB** and **5Te** measured at heating and cooling rates of 10 °C min^{-1}.

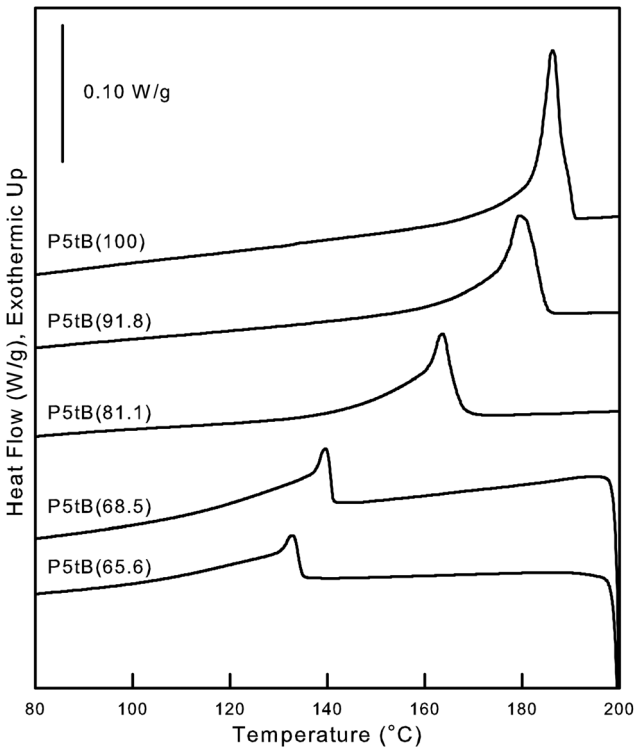

Fig. 2 Cooling DSC traces of the polymers containing at least 65.6 mol% **5tB**. The traces in this plot are the cooling traces from Fig. 1 (cooling rate of 10 °C min^{-1}).

second cooling run. For all of the polymers studied, the heating traces showed a step in the heat flow due to the glass transition in the polymer. The glass transition temperature is lowest for the homopolymer of **5Te** and increases monotonically as more mesogenic diene (**5tB**) is incorporated into the polymer. This trend is attributed to the higher rigidity of **5tB** compared to **5Te**. In addition to this trend in glass transition temperature, the polymers with at least 65.6 mol% **5tB** showed an endotherm in the heating traces at temperatures above T_g (Fig. 1). The polymers that showed an endotherm in the heat also showed an exotherm in the cooling trace, with some supercooling. This endotherm/exotherm pair is due to the clearing (nematic-isotropic) transition in these enantiotropic liquid crystalline polymers. Fig. 1 also shows that not all of the polymers are liquid crystalline: the homopolymer of **5Te** and the **P5tB(40.1)** copolymer did not show an endotherm or exotherm in their heating and cooling traces, respectively. The loss of liquid crystallinity in polymers with lower **5tB** content is attributed to an increase in chain flexibility. In such flexible polymers, the entropic penalty for forming an ordered liquid crystalline phase is greater than the enthalpic gain of forming such a phase and, as such, the flexible chains tend to form an entropically favored coil rather than a chain-extended, ordered LC phase.

To observe the differences in the clearing transition more clearly, Fig. 2 shows the DSC cooling traces from Fig. 1 on expanded heat flow and temperature scales. The isotropic–nematic transition temperature was highest for the homopolymer of **5tB** and decreased with increasing content of the **5Te**.

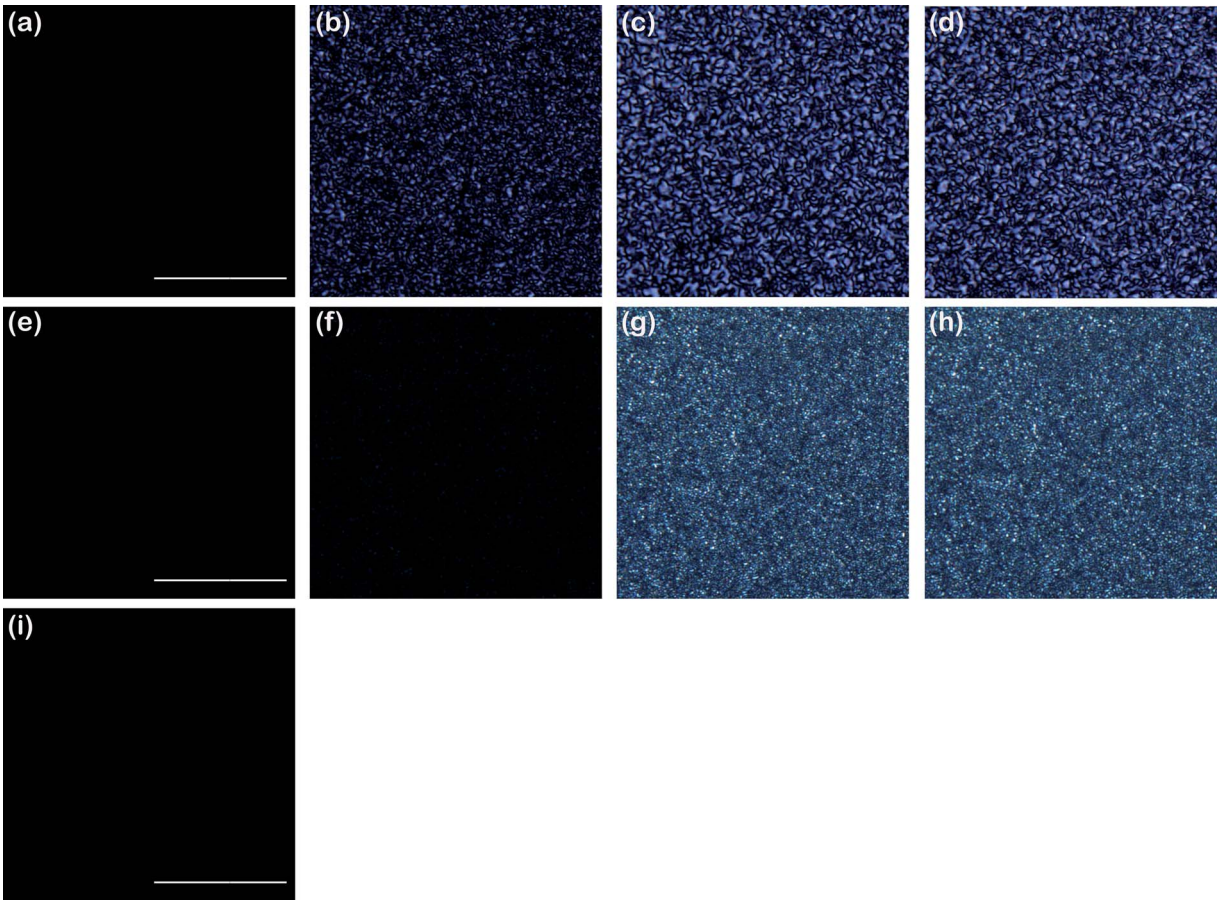

Fig. 3 Polarized light optical microscopy images of **P5tB(100)** (a–d), **P5tB(65.6)** (e–h), and **P5tB(40.1)** (i). The images were acquired while cooling the polymer from the isotropic state at a rate of 10 °C min^{-1}. The **P5tB(100)** images correspond to the following temperatures: (a) 200 °C, (b) 182 °C, (c) 104 °C, and (d) 23 °C. The **P5tB(65.6)** images correspond to the following temperatures: (e) 167 °C, (f) 112 °C, (g) 57 °C, and (h) 30 °C. The **P5tB(40.1)** image shown was acquired at (i) 25 °C. All scale bars are 20 μm.

Qualitatively, this is the same trend displayed by the glass transition temperature. Further examination of these data allows two additional qualitative observations to be made concerning the isotropic–nematic transition. First, as mesogenic monomer decreased in favor of the more flexible comonomer, the latent heat of the isotropic–nematic transition decreased. Second, the shape of the isotropic–nematic transition also changed throughout the series of polymers. The exothermic peak was sharpest for the homopolymer of **5tB**, though it did tail slightly on the low temperature side of the peak, yielding a strongly asymmetric peak. This low temperature tail moved increasingly closer to the peak's maximum as the amount of **5Te** in the polymer increased. The low temperature shoulder was especially pronounced in **P5tB(65.6)**, where the prominent tail faded into the baseline and obscured the low temperature limit of the peak. The decrease in the clearing temperature and broadening of the transition are attributed to the increase in flexibility of the polymer chains due to the increasing fraction of the more flexible comonomer **5Te**. The comonomers may also cause heterogeneity in backbone stiffness, as discussed later.

Hot stage polarized light optical microscopy (POM) was used to further study the transition from isotropic to liquid crystalline state of **P5tB(100)** (Fig. 3(a–d)), **P5tB(65.6)** (Fig. 3(e–h)), and **P5tB(40.1)** (Fig. 3(i)), three polymers that are representative of the series. To image regions of birefringence (liquid crystallinity), the microscope was configured to transmit linearly polarized white light through the sample and then "analyze" the transmitted light using a second linear polarizer after the objective lens, but before the CCD camera. With such a configuration, the transmitted intensity (I/I_o) follows the relation:

$$\frac{I}{I_o} = \sin^2(\pi \Delta n h/\lambda)\sin^2(2\chi) \quad (2)$$

where Δn is the birefringence, h is the optical path length, λ is the light wavelength, and χ is the angle between the incident polarization and the local average orientation (director). As such, regions of liquid crystallinity ($\Delta n > 0$) appear bright, whereas isotropic regions appear dark with $I = 0$ due to a lack of polarized light rotation by the sample.

At 200 °C all of the polymers are in the isotropic phase and thus none of the samples exhibited birefringence in the POM images (Fig. 3(a)). Upon cooling at 10 °C min^{-1}, the samples with at least 65.6 mol% **5tB** in the polymer underwent the isotropic–nematic transition wherein birefringence appeared in a wavelike manner from one end of the sample to the other, reflecting a minor temperature gradient in the sample. Unlike spherulitic

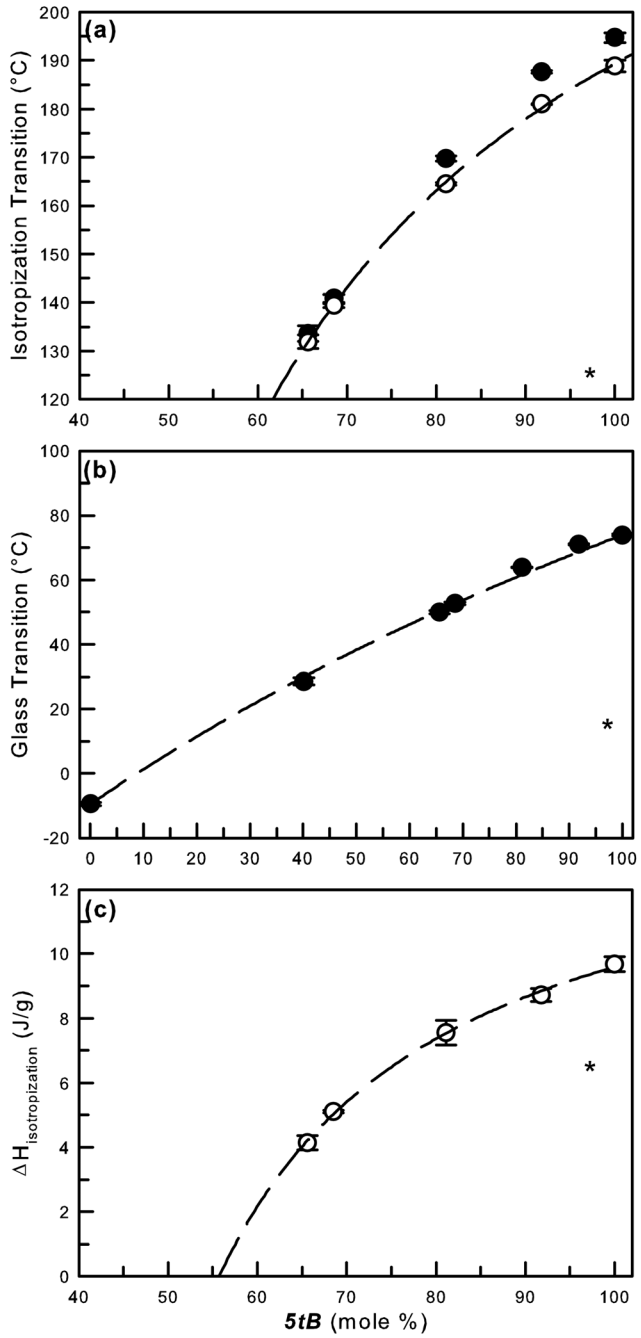

Fig. 4 Average clearing (a) and glass transition (b) temperatures and average latent heat of the clearing transition in the DSC cooling trace (c) plotted as a function of **5tB** content. Values shown are the average from at least four runs, and error bars denote the standard deviation for each point. Filled circles denote data from heating runs, and open circles denote data from cooling runs. The dashed lines are regression fits to the data, as described in the text. The asterisks denote data acquired during the DSC second heating trace of **P5tB(97.3)**.

growth, nucleation was not observed and birefringence did not grow radially, but instead moved as a front across the field of view. The images of **P5tB(100)** in Fig. 3(b–d) show dark brushes meeting at disclinations in the sample. The Schlieren textures aid the identification of the nematic phase, as points where only two brushes converge are only observed in the nematic phase and indicate wedge declination with strength $\pm 1/2$. The thickness of the sample makes the identification of these disclinations more difficult, but upon close inspection of the **P5tB(100)** images several disclinations with only two brushes may be found (Fig. 3(b–d)). This suggests that **P5tB(100)** is nematic upon becoming liquid crystalline, but this may be further confirmed using X-ray analysis to examine the small angle region.[61] As the temperature was reduced further, the isotropic (dark in the POM images) regions of the sample became ordered and the POM image became brighter until a maximum birefringence was reached. **P5tB(40.1)** did not display birefringence at any temperature, confirming the DSC results that this polymer is not liquid crystalline.

While visual inspection of Fig. 1 reveals qualitatively that the glass and clearing transitions both decrease as more **5Te** is incorporated into the polymer, plots of the transition temperatures (Fig. 4) reveal in detail how these transitions change with composition. The clearing temperature (Fig. 4(a)) decreased dramatically as the amount of **5tB** in the polymer decreased. The glass transition temperature obeyed the same trend (Fig. 4(b)), but is shown to decrease more gradually than the clearing transition. It should be noted that there are fewer points in the clearing temperature series compared to the glass transition temperature series because not all of the polymers are liquid crystalline. Fitting of the glass transition data presented in Fig. 4(b)) was possible using the empirical Gordon–Taylor equation (eqn (3)).

$$T_g^{cop} = \frac{w_1 T_{g,1} + k w_2 T_{g,2}}{w_1 + k w_2} \quad (3)$$

The Gordon–Taylor equation was originally developed to describe dependence of the glass transition temperature on blend composition in miscible blends of polymers. The parameter k describes the interactions between the two components, where larger values of k indicate favorable interactions between components.[62,63] Here, mole fraction was used instead of the weight fraction convention because mole fraction was measured directly from ^{1}H NMR. The fit of eqn (3) to the T_g data shown in Fig. 4(b) resulted in a R^2 of 0.998 and a k of 0.747, indicating there may be some favorable interactions between the two monomers.

The latent heat of the clearing transition ($\Delta H_{clearing}$) was measured for the heating and cooling curves and was found to decrease as the amount of **5tB** in the polymer decreased (Fig. 4(c)), an observation that agrees with qualitative observation of the DSC traces from Fig. 1 and 2. Importantly, Fig. 4(c) shows that there is a minimum mole percent of **5tB** required for a liquid crystalline phase to exist in these copolymers, and this critical composition can be determined by finding the x-intercept (composition) through extrapolation of a regression line fit to the data. In the absence of a fundamental expression for this trend, we adopted the rational expression given by eqn (4):

$$\Delta H_{clearing}\left(\mathrm{J\ g^{-1}}\right) = \frac{(1 + a x_{\mathbf{5tB}})}{(b + d x_{\mathbf{5tB}})} \quad (4)$$

where $\Delta H_{clearing}$ is the latent heat (J g^{-1}) of the clearing transition measured from the cooling trace and $x_{\mathbf{5tB}}$ is the mole percent of **5tB** in the polymer. The regression line fits the data well ($R^2 = 0.998$) and the coefficients were determined to be

$a = -1.80 \times 10^{-2}$, $b = 3.53 \times 10^{-2}$, and $d = -1.83 \times 10^{-3}$. The regression fit (dashed line) is shown fit to the data (open circles) in Fig. 4(c). Eqn (4) predicts that at least *ca.* 56 mol% of **5tB** is required for polymers of **5Te** and **5tB** to be liquid crystalline. This value may depend on molecular weight, though this effect was not investigated systematically.

A rational expression of similar form to eqn (4) fit well ($R^2 = 0.999$) to the plot of clearing temperature measured during cooling *versus* **5tB** content in the polymer (Fig. 4(a)) and is given by eqn (5).

$$T_{\text{clearing}}(^\circ\text{C}) = \frac{(1 - 0.025x_{\mathbf{5tB}})}{(0.001 - 8.874 \times 10^{-5}x_{\mathbf{5tB}})} \quad (5)$$

The clearing transition for the hypothetical polymer that has the minimum amount of **5tB** (56 mol%) required for liquid crystallinity is thus predicted to be 99 °C (from eqn (5)), and the glass transition of this polymer is predicted to be 46 °C (from eqn (3)).

The analysis of the data in Fig. 4 highlights our observation that copolymerization of **5tB** with the **5Te** comonomer leads to polymers whose isotropization temperature is reduced more quickly than their glass transition temperature. Crosslinking a polymer usually increases the glass transition temperature. Crosslinks can also hinder liquid crystalline ordering, resulting in a network with a lower clearing temperature and latent heat of clearing than the polymer before crosslinking. Thus, if a liquid crystalline elastomer is desired using this two stage route, the ideal starting polymer would have a strong clearing transition and a low (preferably subambient) glass transition temperature. Such polymers may be prepared by replacing **5Te** with another comonomer that favors T_g depression over clearing point depression. As will be shown later, however, crosslinking a **5tB/5Te** copolymer resulted in the formation of a liquid crystalline elastomer. The low T_g of the network, and thus its elastomeric nature at room temperature, will be attributed to the lower molecular weight of the starting material as well as plasticization of the network by the initiator, itself.

The unsaturated carbon–carbon double bonds in the backbone of all of these polymers may be exploited for free-radical crosslinking using a peroxide initiator. Free-radical crosslinking was demonstrated using **P5tB(97.3)-G3**, a polymer that was synthesized using Grubbs' third generation catalyst. This polymer had 95.3 mol% **5tB** in the feed of the reaction, and the polymer contained 97.3 mol% **5tB** as determined by ^{1}H NMR in $CDCl_3$. The resulting molecular weight of this polymer was lower than the polymers prepared by the methods described above. Specifically, M_w was found to be low at 6.96 kDa, as measured by GPC. The lower molecular weight of these polymers is not thought to be due to the different catalyst, rather it is attributed to the less rigorous control over polymerization atmosphere employed for these syntheses compared to those used for the polymers described above. In fact, this lower molecular weight was desirable for crosslinking, as described later.

The DSC second heating trace of **P5tB(97.3)-G3** showed a T_g of only 13.3 °C (0.381 J g^{-1} °C^{-1}) and a clearing endotherm at 124 °C (4.86 J g^{-1}), while the second cooling trace showed an exotherm at 119 °C (6.31 J g^{-1}) (Fig. 5(a), trace (i)). These data are plotted in Fig. 4(a–c) and are denoted by asterisk symbols (*). Though we have not studied directly the effect of molecular weight on properties, the lower temperatures of the glass and clearing transitions are attributed to the lower molecular weight of this polymer. A cooling sequence of three POM images of this LCP acquired upon cooling from the isotropic state at 10 °C min^{-1} are shown in Fig. 5(b–d). At temperatures above the clearing exotherm observed in the DSC trace, the POM images were black and indicate the polymer is in the isotropic state. At 120 °C, the POM image showed brightness due to liquid crystallinity (Fig. 5(c)), and upon cooling further, the polymer retained its birefringence but did not crystallize (Fig. 5(d)).

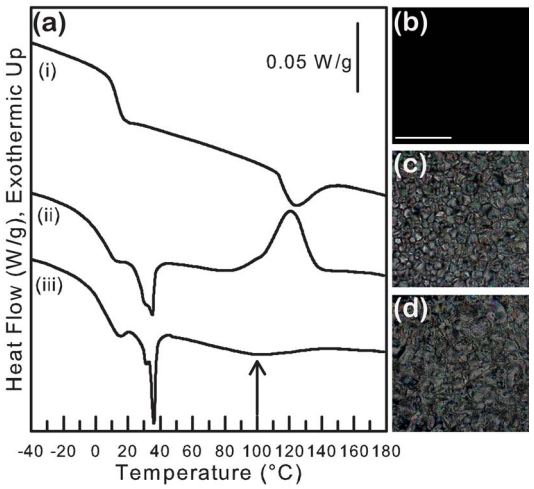

Fig. 5 (a) Free-radical crosslinking of **P5tB(97.3)** blended with 10 wt% lauroyl peroxide. Shown are the DSC heating traces of the (i) polymer before crosslinking and without initiator, (ii) the first heating trace of the polymer and initiator blend after curing at 90 °C for 30 min showing the exotherm due to the completion of the cure, and (iii) the second heat after curing the polymer and initiator blend, showing the glass transition and clearing transition (highlighted by the arrow) of the cured polymer, as well as a melting transition from lauroyl peroxide. (b–d) Polarized light optical microscopy images of **P5tB(97.3)** acquired during a cool from the isotropic state at 10 °C min^{-1} at the following temperatures: (b) 150 °C, (c) 120 °C, and (d) 30 °C. Scale bar denotes 40 μm.

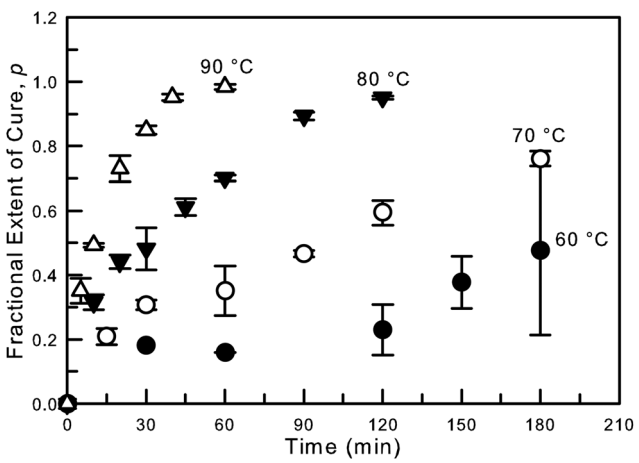

Fig. 6 Extent of cure of **P5tB(97.3)** with 10 wt% lauroyl peroxide. The fractional extent of cure was calculated using eqn (1) and the residual exothermic heat of reaction measured from the first heating trace after crosslinking.

The kinetics of crosslinking **P5tB(97.3)-G3** with 10 wt% lauroyl peroxide was studied using DSC. Fig. 5 shows DSC traces from the second heat of the polymer, **P5tB(97.3)-G3**, without lauroyl peroxide (trace i). The same plot shows the first (trace ii) and second (trace iii) heating traces of **P5tB(97.3)-G3** after it was cured for 30 min at 90 °C with 10 wt% lauroyl peroxide. The endotherms observed in traces (ii) and (iii) at about 39 °C are due to the melting of the initiator, which indicates that some of the lauroyl peroxide was phase separated and able to crystallize independently of the network. This melting endotherm was not observed in DSC experiments on blends containing a smaller initiator loading (5.16 wt%), as is shown below. The large exotherm in trace (ii) is due to the reaction of material that was not completely cured during the prior isothermal cure and was used to calculate the fractional extent of cure, p, from eqn (1) for each of the different cure times and temperatures. Finally, the arrow denoting the endotherm in trace (iii) is due to the clearing transition of the network, which has a minimum at 101 °C and an associated latent heat of 4.46 J g^{-1}.

The extent of cure, p, is plotted *versus* cure time for the four different cure temperatures in Fig. 6. From this data, the rate constant of the cure, $k(T)$, was determined at each temperature, and these rate constants were ultimately used to determine activation energy of the cure using the Arrhenius equation (eqn (6)).

$$\ln\big(k(T)\big) = \ln(A) - \frac{E_a}{RT} \tag{6}$$

Fig. 6 shows that, in the early stages of cure, the extent of reaction increases sharply with increasing cure time and suggests a first order rate dependence. A first order reaction has a linear relationship between the rate of reaction and the fractional extent of cure p, and this differential equation may be solved to give the time dependence of the fractional extent of cure (eqn (7)).

$$\ln(1 - p) = -kt \tag{7}$$

The extent of cure data (Fig. 6) was plotted in the form of the natural logarithm of $(1 - p)$ *versus* cure time, t (see ESI†). Linear regression was applied to the plots of $\ln(1 - p)$ *versus* t at each temperature to determine the rate constants, $k(T)$, for the different temperatures. Only the four shortest cure times at each temperature were used for the regression because some deviation from linearity was observed for the longer cure times, though limited data points prohibit the determination of the cause of this deviation. The data was found to fit well to eqn (7), which suggests that reaction was indeed first order, a finding that is consistent with a previous report where **P5tB(100)** was crosslinked using 10 wt% dicumyl peroxide.[57,61] Table 2 indicates that such linear regression analysis worked reasonably well for the 90 °C ($R^2 = 0.992$) and 80 °C ($R^2 = 0.910$) cures, and moderately well for the 70 °C cure ($R^2 = 0.826$). At 60 °C, the $R^2 = 0.701$ was lower than desired, which we attribute to the low reaction rate that lead to only small changes in $\Delta H_{res}(T,t)$. Finally, the temperature-dependent rate constants ($k(T)$) were plotted *versus* $1/T$ to determine the activation energy for the early stages of the cure using the eqn (6). The R^2 for this regression analysis was 0.999, and from this analysis the activation energy (E_a) of the early stages of the cure was found to be 118.9 kJ mol^{-1}. This value is quite similar to the range of activation energies (126 kJ mol^{-1}–168 kJ mol^{-1}) that were reported from the crosslinking of several polyolefins, including styrene-butadiene rubber, with different peroxide initiators.[64]

Table 2 First-order rate constants from the free-radical crosslinking of **P5tB(97.3)** with 10 wt% lauroyl peroxide. These rate constants were obtained by fitting the natural logarithm of $(1 - p)$ (where p is the fractional extent of cure) *versus* time using linear regression. The four shortest isothermal cure times at each temperature were used for the regression analysis

Temperature (°C)	R^2	$k \times 10^{-3}$ (min^{-1})
90	0.992	6.39
80	0.910	2.17
70	0.826	0.679
60	0.701	0.183

The time required for network gelation depends on the kinetics of the reaction and will decrease with increasing temperature or initiator loading. As discussed above, it was desired to reduce the initiator concentration from 10 wt% to 5.16 wt% for rheology experiments to reduce gas bubbles that could form from lauroyl peroxide decomposition. A DSC curing kinetics study was thus conducted on **P5tB(97.3)-G3** blended with 5.16 wt% lauroyl peroxide to provide insight on the extent of reaction reached by rheology samples. These samples were cured in DSC pans on a hot stage at 60 °C for varying lengths of time before analyzing using DSC. The first heating after curing allowed measurement of the residual heat of reaction, ΔH_{res}, from the area under the exotherm, and this was compared to an uncured sample of **P5tB(97.3)-G3** blended with 5.16 wt% lauroyl peroxide. The extent of reaction for different cure times at 60 °C is shown in the Fig. 7. The data was plotted in the form described by eqn (7), and the regression line fit to this plot was found to fit the data well ($R^2 = 0.983$) with a rate constant, k, of 0.186 h^{-1}. Interestingly, in contrast to **P5tB(97.3)-G3** cured with 10 wt% lauroyl peroxide, no endothermic transition from lauroyl peroxide melting was observed in the second heating trace after completion of cure.

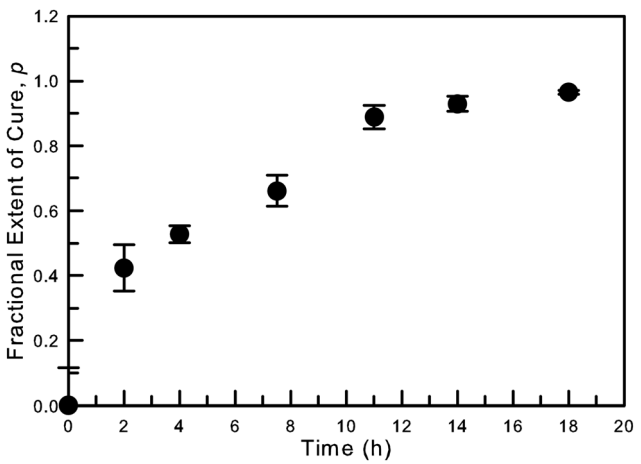

Fig. 7 Free-radical crosslinking of **P5tB(97.3)-G3** with 5.16 wt% lauroyl peroxide at 60 °C. The fractional extent of cure was calculated using eqn (1) and the residual exothermic heat of reaction measured from the first heating trace after crosslinking.

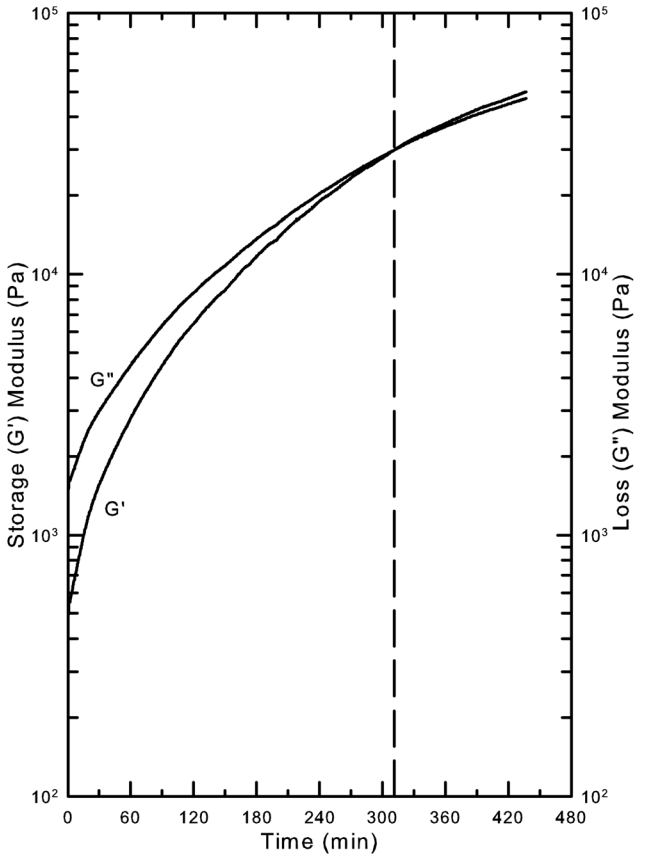

Fig. 8 Small angle oscillatory shear rheology of **P5tB(97.3)** blended with 5.16 wt% lauroyl peroxide. The sample was loaded at 60 °C in between 8 mm parallel plates, and sheared at 1% strain and 10 rad s^{-1} during the isothermal hold. The storage modulus, G', and loss modulus, G'', for the entire time sweep are shown.

This finding indicates that lauroyl peroxide crystallizes independent from the network at 10 wt%, but that the 5.16 wt% loading may be miscible with the network.

While calorimetry allowed the crosslinking kinetics to be determined, further proof that lauroyl peroxide crosslinks **P5tB(97.3)-G3** was obtained using parallel plate rotational rheometry. Upon thermal decomposition, as is necessary for radical formation, lauroyl peroxide forms gaseous byproducts, which can become trapped in the sample during crosslinking. Thus, for these experiments, **P5tB(97.3)-G3** was blended with a lower concentration (compared to the multi-temperature kinetics study) of 5.16 wt% lauroyl peroxide. Fig. 8 shows the evolution of dynamic storage and loss moduli during an isothermal time sweep at 60 °C. Initially, the loss modulus was larger than the storage modulus, but, as the isothermal cure continued, the storage modulus increased more quickly than the loss modulus. This difference in the rate of change of the moduli resulted in the storage modulus crossing the loss modulus at a point taken to be the gel point. Once the gel point is reached, the sample is more elastic than it is viscous, indicating that a network has formed.

For the experiment shown, the time to gelation is 311 minutes and is marked by the vertical dashed line. It should be noted that not all bubble formation was suppressed by reducing the initiator loading, thus the moduli reported in Fig. 8 are likely smaller than

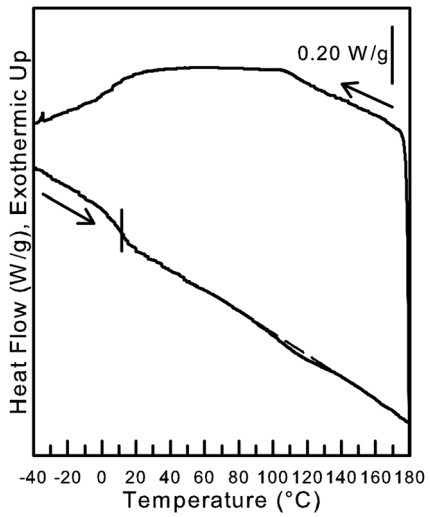

Fig. 9 DSC of **P5tB(97.3)-G3** crosslinked with 5.16 wt% lauroyl peroxide at 60 °C for 7.28 h during small angle oscillatory shear in a parallel plate rheometer. Shown are the second heating and second cooling traces of the resulting network, both of which were measured using heating and cooling rates of 10 °C min^{-1}. The vertical line marks T_g, and the dashed line is a linear regression fit ($R^2 = 0.999$) to the heat flow signal added to highlight the isotropization endotherm.

what would be measured if no gas bubbles formed. Comparing the time to gelation to the kinetics data shown in Fig. 7 and the corresponding regression analysis, the sample shown in Fig. 8 is estimated to have an extent of cure of 0.62 when the storage modulus crossed the loss modulus; *i.e.* at the gel point. The extent of cure at the gel point varies widely based on the functionality of the reagents.[65–67] A model proposed by Carothers[68] predicts the extent of cure at the gel point, p_c, using the average functionality of the crosslinker, $\bar{f}$. (eqn (8))

$$p_c = \frac{2}{\bar{f}} \tag{8}$$

Using 0.62 as the extent of cure at the gel point leads to an effective functionality of 3.2, which is smaller than the calculated functionality of 12.4 (by ^{1}H NMR) for **P5tB(97.3)-G3**. The difference between the effective and the calculated functionality means that not every double bond in the polymer reacted to form a crosslink, which is thought to be caused by geometric constraints.

Finally, Fig. 9 shows the second heating and second cooling DSC traces of **P5tB(97.3)-G3** crosslinked in the rheometer. These results support a qualitative assessment from mechanical manipulation that the material is an elastomer, showing a sub-ambient T_g at 11.4 °C (0.601 J g^{-1} °C^{-1}). Further, the results suggest that the network is liquid crystalline with a broad clearing transition at 115 °C (3.38 J g^{-1}) in the heating trace and a somewhat sharper exotherm at 106 °C (2.65 J g^{-1}) in the cooling trace. Not surprisingly, the liquid crystalline phase of the network is less stable than **P5tB(97.3)-G3**, as demonstrated by the comparing the latent heat of the clearing transition for the **P5tB(97.3)-G3** polymer to the crosslinked network. While the endotherm and exotherm pair suggests that this elastomer is liquid crystalline, additional techniques such as hot stage

microscopy or X-ray scattering would aid in confirming this result.

Discussion

Both the temperature and the latent heat of the clearing transition were observed to reproducibly decrease as **5tB** content in the polymer decreased. These observations can be understood by considering the differences in the rigidity of the monomers and homopolymers of **5tB** and **5Te**. Considering the monomers first, **5tB** is a rigid molecule that exceeds the aspect ratio required for liquid crystallinity, whereas **5Te** has a shorter aromatic core and thus does not have the required aspect ratio. Once polymerized, the homopolymer of **5Te** favors coiling at all temperatures because its persistence length is sufficiently short. The **5tB** homopolymer, in contrast, does not favor adoption of a coiled conformation below the clearing transition because its persistence length is larger. Instead, the **5tB** homopolymer favors an extended conformation, and there is an enthalpic driving force for the chains to condense to a liquid crystalline phase. If the polymer is heated through its isotropization transition, entropy will overwhelm enthalpy, and the polymer chain will collapse into a coil, causing the material to transition to an isotropic phase.

Researchers have shown that changing the rigidity of a copolymer affects its clearing transition, with two separate reports discussed here briefly. Stupp and coauthors[30,31,33] compared regiorandom to regioregular liquid crystalline copolyesters and found that the regular polymer's crystals melt into a liquid crystalline phase by passing through a sharper transition at a higher temperature than the random polymer's crystals melt. The differences in the phase behavior of these polymers were attributed to a less perfect molecular organization in the random polymer, which is more easily disrupted than in the ordered system. This hypothesis was further studied by simulation[31] of these polymers, where it was found that the compositional disorder of the system leads to a distribution in the polymers' persistence lengths (calculated as "rigidity factors"), and results in the broadening of the melting transition in the random polymer. Pavel and coauthors[69] studied the effect of comonomer sequence by simulation using monomer units with varying degrees of rigidity. The found, not surprisingly, that the nematic to isotropic transition was related to the persistence ratio of the polymer, q/d, where q is defined as the persistence length and d is defined as the maximum diameter of the chain. As described above, the polymers adopt a coiled conformation in the isotropic state and thus have a lower persistence length than in the nematic state. Pavel *et al.* adopted the convention[69] that the clearing transition is characterized by a q/d of 5 and found that, by calculating q/d at different temperatures, the nematic to isotropic transition of different monomer sequences could be determined. They found that incorporating flexible monomer units decreases the rigidity of the polymer chain and leads to a drop on the nematic to isotropic transition temperature. While the methods by which these simulations were conducted do differ, the end results are similar in that they predict that decreasing the rigidity of the chain will decrease the polymer's persistence length and thus the temperatures at which the nematic phase is stable. Stupp has further reported that disorder introduced by the variation in persistence lengths also destabilizes the nematic phase. From these previous reports, we suggest that the reduction in the temperature and latent heat of the isotropization transition in the copolymers are due to the more flexible comonomer (**5Te**), which decreases the polymer's persistence length and increases disorder by its random distribution within the polymer chain. Currently, no modeling studies addressing both the glass transition and the isotropization transition have been reported.

An advantage of preparing networks in the two step fashion we adopted here is that one can vary the properties of the polymer prior to crosslinking, thus providing an additional level at which the properties of the networks may be controlled. Because ADMET chemistry was used to polymerize these monomers, the resulting polymers contained unsaturated sites available for free-radical crosslinking. Here, the polymers were crosslinked in a liquid crystalline phase using lauroyl peroxide. Lauroyl peroxide was selected for its low initiation temperature, which permitted rheological experiments to be conducted at a temperature low enough (close enough to T_g) to afford a viscosity that will support a meniscus in rotational rheometry. While a low molecular weight polymer was challenging for the rheological experiments, it is desirable for crosslinking because diffusion is less hindered by melt viscosity. Furthermore, low viscosity of reactive oligomers or polymers is desirable for the composite manufacturing process, resin transfer molding (RTM). The networks shown here are liquid crystalline and elastomeric with a glass transition temperature of 11.4 °C, nearly 2 °C lower than the polymer prior to crosslinking. Because T_g did not increase upon crosslinking, lauroyl peroxide and the products formed during initiation are thought to act as plasticizers. Two different initiator loadings were studied, and it was found that the lower initiator loading (~5 wt%) did not melt or crystallize independently from the network, but that a melting transition could be detected by DSC when the initiator loading was doubled. The two initiator concentrations are thought to bracket the miscibility limit for lauroyl peroxide in the polymer, where the lower initiator loading was miscible with the network but the higher loading was not. Here, the miscibility of the initiator with the network was combined with a low T_g liquid crystalline polymer to yield a liquid crystalline elastomer, the first non-siloxane main-chain LC elastomer, to our knowledge.

Conclusions

This study demonstrated that the glass and clearing transitions of a main-chain thermotropic liquid crystalline polymer can be controlled by copolymerizing with a flexible comonomer. Here, the clearing transition was found to decrease more dramatically than the glass transition temperature as mesogen content was lowered. The decrease in clearing temperature and latent heat of clearing in compositions that include a lower mesogen concentration were explained to be an effect of decreasing persistence length in the polymer as well as disorder effects arising from the random incorporation of the monomers. Crosslinking through the unsaturated bonds in the polymer chain was shown to be an effective way to create networks, though the stability of the liquid crystalline phase was reduced upon crosslinking. Finally, crosslinking of a selected composition was shown to result in the formation of a liquid crystalline elastomer. The elastomeric

properties of this network were attributed to be due to the low T_g of the polymer and some miscibility of the initiator with the polymer network.

Acknowledgements

The authors are grateful for the support of the National Science Foundation. PTM acknowledges support from National Science Foundation (DMR-0758631 and DMR-1004807). KAB acknowledges the support of a Graduate Research Fellowship from the National Science Foundation (DGE-0234629).

References

1 J.-I. Jin and C.-S. Kang, *Prog. Polym. Sci.*, 1997, **22**, 937–973.
2 C. Noel and P. Navard, *Prog. Polym. Sci.*, 1991, **16**, 55–110.
3 S. S. Kim and C. D. Han, *Macromolecules*, 1993, **26**, 3176–3186.
4 S. S. Kim and C. D. Han, *J. Rheol.*, 1993, **37**, 847–866.
5 P. T. Mather, A. Romo-Uribe, C. D. Han and S. S. Kim, *Macromolecules*, 1997, **30**, 7977–7989.
6 P. T. Mather, H. G. Jeon, C. D. Han and S. Chang, *Macromolecules*, 2000, **33**, 7594–7608.
7 C. D. Han and S. S. Kim, *Macromolecules*, 1995, **28**, 2089–2092.
8 W. J. Jackson, Jr, *Br. Polym. J.*, 1980, **12**, 154–162.
9 W. J. Jackson, Jr, *Contemp. Top. Polym. Sci.*, 1984, **5**, 177–208.
10 W. Heitz and N. Neibner, *Makromol. Chem.*, 1990, **191**, 225–235.
11 P. K. Bhowmik and H. Han, *Macromolecules*, 1993, **26**, 5287–5294.
12 R. A. Gaudiana, R. A. Minns, R. Sinta, N. Weeks and H. G. Rogers, *Prog. Polym. Sci.*, 1989, **14**, 47–89.
13 P. Mather, N. Grizzuti, G. Heffner, M. Ricker, W. E. Rochefort, M. Seitz, H. W. Schmidt and D. S. Pearson, *Liq. Cryst.*, 1994, **17**, 811–826.
14 W. J. Jackson, Jr and J. C. Morris, US 4 169 933, 1979.
15 A. J. East and G. W. Calundann, (Celanese Corp., USA). US 4 318 841, 1982, p. 8.
16 J. Majnusz, J. M. Catala and R. W. Lenz, *Eur. Polym. J.*, 1983, **19**, 1043–1046.
17 H.-R. Dicke and R. W. Lenz, *J. Polym. Sci., Polym. Chem. Ed.*, 1983, **21**, 2581–2588.
18 M. Ballauff, *Makromol. Chem., Rapid Commun.*, 1986, **7**, 407–414.
19 J. Watanabe, B. R. Harkness, M. Sone and H. Ichimura, *Macromolecules*, 1994, **27**, 507–512.
20 R. M. Rodriguez-Parada, R. Duran and G. Wegner, *Macromolecules*, 1989, **22**, 2507–2516.
21 C.-S. Kang, C. Heldmann, H.-J. Winkelhahn, M. Schulze, D. Neher, G. Wegner, R. Wortmann, C. Glania and P. Kramer, *Macromolecules*, 1994, **27**, 6156–6162.
22 S. B. Damman, F. P. M. Mercx and C. M. Kootwijk-Damman, *Polymer*, 1993, **34**, 1891–1897.
23 W. Brugging, U. Kampschulte, H.-W. Schmidt and W. Heitz, *Makromol. Chem.*, 1988, **189**, 2755–2767.
24 W. Heitz and H.-W. Schmidt, *Makromol. Chem., Macromol. Symp.*, 1990, **38**, 149–160.
25 R. W. Lenz and J.-I. Jin, *Macromolecules*, 1981, **14**, 1405–1411.
26 R. Cai, J. Preston and E. T. Samulski, *Macromolecules*, 1992, **25**, 563–568.
27 R. Cai and E. T. Samulski, *Macromolecules*, 1994, **27**, 135–140.
28 R. Cai and E. T. Samulski, *Liq. Cryst.*, 1991, **9**, 617–634.
29 W. R. Krigbaum, R. Kotek, T. Ishikawa and H. Hakemi, *Eur. Polym. J.*, 1984, **20**, 225–235.
30 P. G. Martin and S. I. Stupp, *Macromolecules*, 1988, **21**, 1222–1227.
31 S. I. Stupp, J. S. Moore and P. G. Martin, *Macromolecules*, 1988, **21**, 1228–1234.
32 J. S. Moore and S. I. Stupp, *Macromolecules*, 1987, **20**, 273–281.
33 J. S. Moore and S. I. Stupp, *Macromolecules*, 1988, **21**, 1217–1221.
34 H. Hoshino, J.-I. Jin and R. W. Lenz, *J. Appl. Polym. Sci.*, 1984, **29**, 547–554.
35 A. Shiota and C. K. Ober, *Prog. Polym. Sci.*, 1997, **22**, 975–1000.
36 E. P. Douglas, *Polym. Rev.*, 2006, **46**, 127–141.
37 C. Ortiz, R. Kim, E. Rodighiero, C. K. Ober and E. J. Kramer, *Macromolecules*, 1998, **31**, 4074–4088.
38 C. Ortiz, L. Belenky, C. K. Ober and E. J. Kramer, *J. Mater. Sci.*, 2000, **35**, 2079–2086.
39 G. G. Barclay and C. K. Ober, *Prog. Polym. Sci.*, 1993, **18**, 899–945.
40 S. M. Kelly, *J. Mater. Chem.*, 1995, **5**, 2047–2061.
41 J. Schatzle, W. Kaufhold and H. Finkelmann, *Makromol. Chem.*, 1989, **190**, 3269–3284.
42 M. Bispo, D. Guillon, B. Donnio and H. Finkelmann, *Macromolecules*, 2008, **41**, 3098–3108.
43 A. R. Tajbakhsh and E. M. Terentjev, *Eur. Phys. J. E: Soft Matter Biol. Phys.*, 2001, **6**, 181–188.
44 D. L. Thomsen, P. Keller, J. Naciri, R. Pink, H. Jeon, D. Shenoy and B. R. Ratna, *Macromolecules*, 2001, **34**, 5868–5875.
45 C. Ortiz, K. B. Wagener, N. Bhargava, C. K. Ober and E. J. Kramer, *Macromolecules*, 1998, **31**, 8531–8539.
46 M. Tokita, H. Tagawa, H. Niwano, K. Osada and J. Watanabe, *Jpn. J. Appl. Phys., Part 1*, 2006, **45**, 1729–1733.
47 P.-G. de Gennes, *C. R. Acad. Sci., Ser. IIb: Mec., Phys., Chim., Astron.*, 1997, **324**, 343–348.
48 I. A. Rousseau and P. T. Mather, *J. Am. Chem. Soc.*, 2003, **125**, 15300–15301.
49 I. A. Rousseau, in *Chemical Engineering*, University of Connecticut, Storrs, 2004.
50 K. A. Burke and P. T. Mather, *J. Mater. Chem.*, 2010, **20**, 3449–3457.
51 I. A. Rousseau, H. Qin and P. T. Mather, *Macromolecules*, 2005, **38**, 4103–4113.
52 H. Qin, B. J. Chakulski, I. A. Rousseau, J. Chen, X.-Q. Xie, G. S. Constable, P. T. Mather and E. B. Coughlin, *Macromolecules*, 2004, **37**, 5239–5249.
53 J. E. Schwendeman, A. C. Church and K. B. Wagener, *Adv. Synth. Catal.*, 2002, **344**, 597–613.
54 J. A. Love, J. P. Morgan, T. M. Trnka and R. H. Grubbs, *Angew. Chem., Int. Ed.*, 2002, **41**, 4035–4037.
55 J. T. Patton, J. M. Boncella and K. B. Wagener, *Macromolecules*, 1992, **25**, 3862–3867.
56 B. M. McKenzie, R. J. Wojtecki, K. A. Burke, C. Zhang, A. Jakli, P. T. Mather and S. J. Rowan, *Chem. Mater.*, 2011, **23**, 3525–3533.
57 H. Qin, in *Chemical Engineering*, University of Connecticut, Storrs, 2004.
58 P. J. Flory, *Principles of Polymer Chemistry*, Cornell University, Ithaca, 1953.
59 F. Chambon and H. H. Winter, *Polym. Bull.*, 1985, **13**, 499–503.
60 H. H. Winter and F. Chambon, *J. Rheol.*, 1986, **30**, 367–382.
61 H. Qin and P. T. Mather, *Macromolecules*, 2009, **42**, 273–280.
62 M. Gordon and J. S. Taylor, *J. Appl. Chem.*, 1952, **1952**, 493–500.
63 G. Belorgey, M. Aubin and R. E. Prud'homme, *Polymer*, 1982, **23**, 1051–1056.
64 N. Ashikari, T. Kanemitsu, S. Kobayashi, Y. Tajima and T. Kawashima, *Kenkyu Jitsuyoka Hokoku - Denki Tsushin Kenkyusho*, 1969, **18**, 225–241.
65 W. T. Yang, J. Y. Deng and G. T. Jin, *Polym. Bull.*, 1994, **33**, 733–740.
66 S. Mortimer, A. J. Ryan and J. L. Stanford, *Macromolecules*, 2001, **34**, 2973–2980.
67 Y. Ishii and A. J. Ryan, *Macromolecules*, 2000, **33**, 167–176.
68 W. H. Carothers, *Trans. Faraday Soc.*, 1936, **32**, 39–49.
69 D. Pavel, I. Yarovsky and R. Shanks, *Polymer*, 2005, **46**, 2003–2010.

